

Phase Separation-Promoted Redox Deracemization of Secondary Alcohols over a Supported Dual Catalysts System

Zhitong Zhao,^[a] Chengyi Wang,^[a] Qipeng Chen,^[a] Yu Wang,^[a] Rui Xiao,^[a] Chunxia Tan,^{*[a]} and Guohua Liu^{*[a]}

Unification of oxidation and reduction in a one-pot deracemization process has great significance in the preparation of enantioenriched organic molecules. However, the intrinsic mutual deactivation of oxidative and reductive catalysts and the extrinsic incompatible reaction conditions are unavoidable challenges in a single operation. To address these two issues, we develop a supported dual catalysts system to overcome these conflicts from incompatibility to compatibility, resulting in an efficient one-pot redox deracemization of secondary alcohols. During this transformation, the TEMPO species onto the outer surface of silica nanoparticles catalyze the oxidation of racemic alcohols to ketones, and the chiral Rh/diamine species

in the nanochannels of the thermoresponsive polymer-coated hollow-shell mesoporous silica enable the asymmetric transfer hydrogenation (ATH) of ketones to chiral alcohols. To demonstrate the general feasibility, a series of orthogonal oxidation/ATH cascade reactions are compared to prove the compatible benefits in the elimination of their deactivations and the balance of the cascade directionality. As presented in this study, this redox deracemization process provides various chiral alcohols with enhanced yields and enantioselectivities relative to those from unsupported dual catalysts systems. Furthermore, the dual catalysts can be recycled continuously, making them an attractive feature in the application.

Introduction

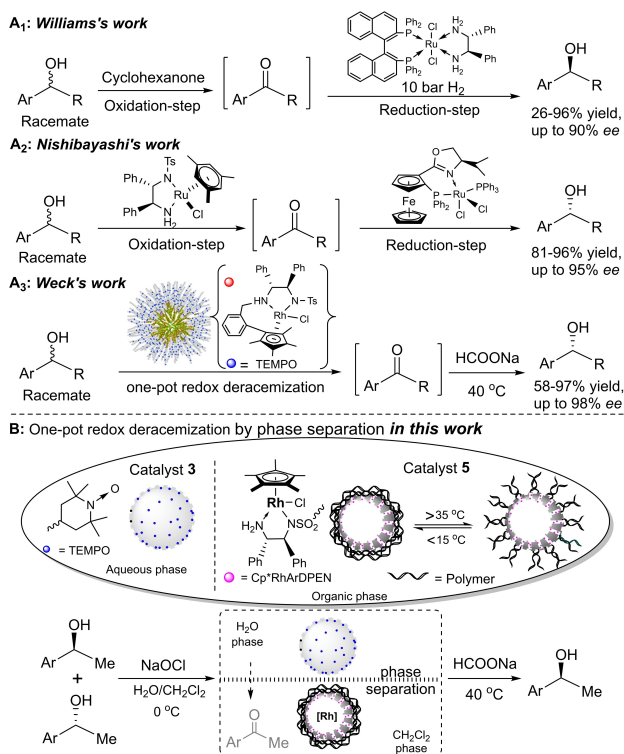
Deracemization represents a promising method for the construction of enantioenriched organic molecules, wherein a racemic mixture can be ideally transformed into two single enantiomers.^[1] Recent studies have presented some notable examples for deracemizations, involving photocatalyst,^[2] enzymes,^[3] supramolecular interactions,^[4] and so on.^[5] Despite its attractiveness, successful deracemizations through a sequential chemical process in a single operation remain challenging.^[6] Optically pure alcohols, as important synthetic motifs, have been used extensively in the pharmaceutical, agrochemical, and fine chemical industries.^[7] Generally, a biocatalytic system through an enzymatic redox deracemization of racemic alcohols can prepare enantioenriched alcohols.^[8] However, due to the restricted substrate specificity of enzymes, a chemical redox deracemization is highly desirable. An ideally chemical transformation, the oxidation of racemic alcohols to ketones and the reduction of ketones to chiral alcohols, can greatly broaden the applications in the construction of enantioenriched alcohol

products. However, this sequential oxidation/reduction process is thermodynamically unfavorable, involving a decreased entropic cost by converting two racemic alcohols into a single alcohol and a kinetically microscopic reversibility used in thermal reactions. Therefore, to obtain an efficient redox deracemization process, two obligatory events must be overcome. The first is that the oxidation and reduction work independently to avoid the quench between oxidants and reductants since it is thermodynamically favorable. The second is that this cascade process must match a kinetic demand of the microscopic reversibility, which requires an additional driving force to impart on reaction directionality.

Upon examining the reported redox deracemizations to overcome these drawbacks as shown in Scheme 1,^[9] the William group designed a two-step operation to solve this thermodynamic problem. The initial non-selective oxidation of achiral alcohol using cyclohexanone as a hydrogen acceptor and the subsequent asymmetric hydrogenation with the *in-situ* generated Noyori complex as a catalyst can produce chiral alcohols (Scheme 1A₁).^[9a,b] Meanwhile, the Nishibayashi group also used a similar method to perform this redox deracemization *via* a combination of two chiral ruthenium catalysts (Scheme 1A₂).^[9c] By utilizing a site-isolated method,^[10] the Weck group elegantly assembled TEMPO (2,2,6,6-tetramethylpiperidine-*N*-oxyl) and chiral diamine-based Rh-complex within the different parts of cross-linked micelles to construct a supported catalyst (Scheme 1A₃).^[9d,10d] which enabled an efficient redox deracemization in a one-step operation. But, due to the complicated preparation procedure, it is highly desirable to explore a new method for a highly efficient redox deracemization in a single operation.

[a] Z. Zhao, C. Wang, Q. Chen, Y. Wang, R. Xiao, C. Tan, Prof. G. Liu
International Joint Laboratory on Resource Chemistry of
Ministry of Education
Shanghai Engineering Research Center of
Green Energy Chemical Engineering
Shanghai Normal University
Shanghai 200234 (P. R. China)
Fax: (+) (0086) 216432280
E-mail: tanhx@shnu.edu.cn
ghliu@shnu.edu.cn

Supporting information for this article is available on the WWW under
<https://doi.org/10.1002/cctc.202100738>



Scheme 1. (A) Reported redox deracemizations and (B) a schematic illustration for one-pot redox deracemization in this work

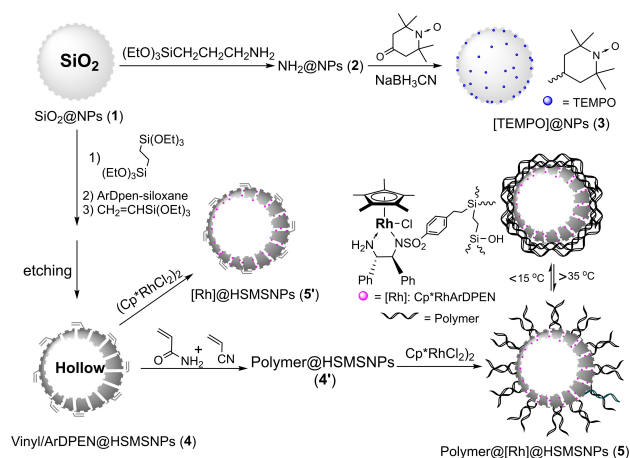
Inspired by a compartmentalization-featured dual catalysts system in our previous report,^[10c] we hypothesize that the phase separation of the biphasic co-solvents in a dual catalysts system can drive a redox deracemization of secondary alcohols to chiral alcohols, wherein two heterocatalysts have different hydrophilicity/hydrophobicity (Scheme 1B). During this transformation, the *in-situ* generated organic ketones *via* an oxidation process of alcohols in the aqueous phase (H₂O phase) could be pumped into the ATH process in the organic phase (CH₂Cl₂ phase). If both oxidant and/or reductant keep enough low concentrations in its corresponding opposite solvent, it can ensure the oxidation and reduction reactions work independently, thereby leading to the desirable chiral alcohols. Herein, we report a rational design of a compartmentalization-type supported dual catalysts system with the hydrophilic supported TEMPO as an oxidative catalyst, and the hydrophobic supported chiral Rh/diamine as a reductive catalyst. As we envisage, the TEMPO species on the outer surface of mesoporous silica nanoparticles can catalyze the oxidation of racemic secondary alcohols into ketones, and the chiral Rh/diamine-species within the nanochannels of the thermoresponsive polymer-coated hollow-shell mesoporous silica nanoparticles can convert the *in-situ* generated ketones into chiral alcohols. Furthermore, the polymer-coating layer in the latter catalyst also offers an additional thermoresponsive driving force to impart on the cascade directionality, meeting a kinetic match of the chiral alcohols to promote this deracemization process. As presented in this study, this phase separation-promoted redox deracem-

ization of secondary alcohols provides various secondary alcohols with enhanced yields and enantioselectivities compared with those from unsupported dual catalysts systems.

Results and Discussion

Syntheses and Structural Characterizations of the Heterogeneous Catalysts

A simple procedure for the anchoring of the TEMPO species onto the outer surface of the silica nanoparticles, abbreviated as [TEMPO]@NPs (3) (TEMPO:^[11a] 2,2,6,6-tetramethylpiperidine-*N*-oxyl), was performed *via* a postgrafting process, as outlined in Scheme 2. Firstly, the silica nanoparticles (SiO₂@NPs (1)) were obtained according to the reported method.^[11a] 3-(triethoxysilyl) propanamine was then postgrafted in the outer surface of the nanoparticles to produce NH₂@NPs (2), followed by the reductive amination with 4-oxo-TEMPO in the presence of NaBH₃CN, affording the crude 3.^[11a] Finally, this crude material was subjected to strict Soxhlet extraction for the removal of the unreacted reagents to give the pure catalyst 3 as a white powder. A thermogravimetric (TG) analysis showed that the propyl-linked TEMPO-loading amounts were 4.79% (see Figure S1 of ESI). Solid-state ¹³C cross-polarization/magic angle spinning (CP/MAS) NMR spectroscopy (see Figure S2 of ESI) disclosed the successful immobilization of TEMPO species onto the outer surface of silica nanoparticles. Besides general signals observed at $\delta = 12.5, 29.7, \text{ and } 46.5$ ppm for the chained alkyl carbon atoms in the propyl moiety, the characteristic signals at δ between 59.4 and 65.3 ppm corresponded to the carbon atoms connected with the nitrogen atoms in the cyclic TEMPO moiety, whereas those at $\delta = 19.5$ and 26.1 ppm could be ascribed to the chained or cyclic alkyl carbon atoms without connection to the nitrogen atoms. All these observations demonstrated the well-defined single-site TEMPO active species because these chemical shifts were the same as those reported in the literature.^[11b] In addition, the silicate network and composition of catalyst 3 were proven by the solid-state ²⁹Si



Scheme 2. Assembly of catalysts 3 and 5 used in the dual catalysts system.

MAS NMR spectroscopy, wherein **3** possessed an inorganic silica network with the strongest Q^3 species ($RO-Si(OSi)_3$; R = propyl-linked TEMPO groups) as its main silica wall of the silica nanoparticles (see Figure S3 of ESI).^[12]

Immobilization of the chiral rhodium/diamine-species within the nanochannels of the silica shell in the water-soluble thermoresponsive polymer-coating hollow-shell mesoporous silica nanoparticles, abbreviated as Polymer@[Rh]@HSMSNPs (**5**) (Polymer:^[13] poly(ethene-co-acrylamide-co-acrylonitrile), [Rh] = $Cp^*RhArDPEN$:^[14] Cp^* = pentamethyl cyclopentadiene, ArDPEN = (S,S)-4-((trimethoxysilyl)ethyl)phenylsulfonyl-1,2-diphenylethylene-diamine), was performed via a sequential polymerization-coordination procedure (Scheme 2). In the free-radical polymerization step, the obtained as-made **4** reacted with acrylamide and acrylonitrile to produce the polymer-coating material Polymer@HSMSNPs (**4'**),^[10c] wherein the polymer-loading amounts were 2.01 %, as determined by the TG analysis (see Figure S4 of ESI). In the coordination step, the reaction of **4'** and $(Cp^*RhCl_2)_2$ at 40 °C in CH_2Cl_2 formed a coarse catalyst, wherein a strict Soxhlet extraction afforded a pure catalyst **5** as a light-yellow powder (see Figure S5 of ESI). For comparison, a parallel analog (**5'**) of the catalyst without the outer polymer-coating layer, abbreviated as [Rh]@HSMSNPs (**5'**), was also prepared following a similar coordination procedure (see experimental part of ESI).

Figure 1 showed the solid-state ^{13}C CP/MAS NMR spectra of **4** and **5**, which revealed the well-defined single-site rhodium/diamine centers within the silica shell in **5**. In general, catalyst **5** presented some common signals observed at $\delta = 192.4$ and 8.4 ppm, corresponding to the carbonyl carbon atoms of the polymeric moiety and the ethyl carbon atoms of the ethane-bridged organic silica, respectively. In particular, catalyst **5** exhibited some characteristic signals at $\delta = 13.0$ and 99.4 ppm, which were ascribed to the methyl and aromatic carbon atoms in the Cp^* ring. These observed characteristic signals were similar to those attained with the corresponding parent $Cp^*RhTsDPEN$,^[14a] proving the well-defined single-site rhodium/diamine centers in **5**. Furthermore, the other carbon signals

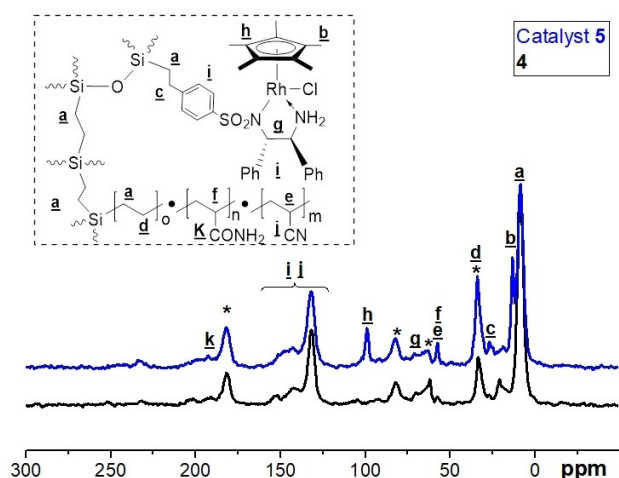


Figure 1. Solid-state ^{13}C CP/MAS NMR spectra of **4** and catalyst **5**.

denoted at asterisk could be assigned to the spinning sidebands for the phenyl group and the alkyl carbon atoms of the residual structure-directing molecules. Moreover, the solid-state ^{29}Si MAS NMR spectra also confirmed its organic silica network, wherein the silica wall in **5** was mainly comprised of the strongest T^3 species ($R-Si(OSi)_3$; R = ethylene-bridged groups and alkyl-linked Ru/diamine complexes) owing to the obviously strong T signals relative to Q signals (see Figure S3 of ESI).

The hollow-shell-structured morphology of the catalyst **5** with ordered pore arrangements was further characterized using scanning electron microscopy (SEM) and transmission electron microscopy (TEM), as shown in Figure 2. The SEM image revealed that the nanoparticles in **5** were uniformly dispersed with an average size of 385 nm (Figure 2a) (also see Figure S6 of ESI for the SEM image of **3**). The TEM image of **5** also disclosed that each silica nanosphere consisted of a nanocage with an average size of 275 nm in diameter and a thin shell of 55 nm in thickness (Figure 2b). In particular, the

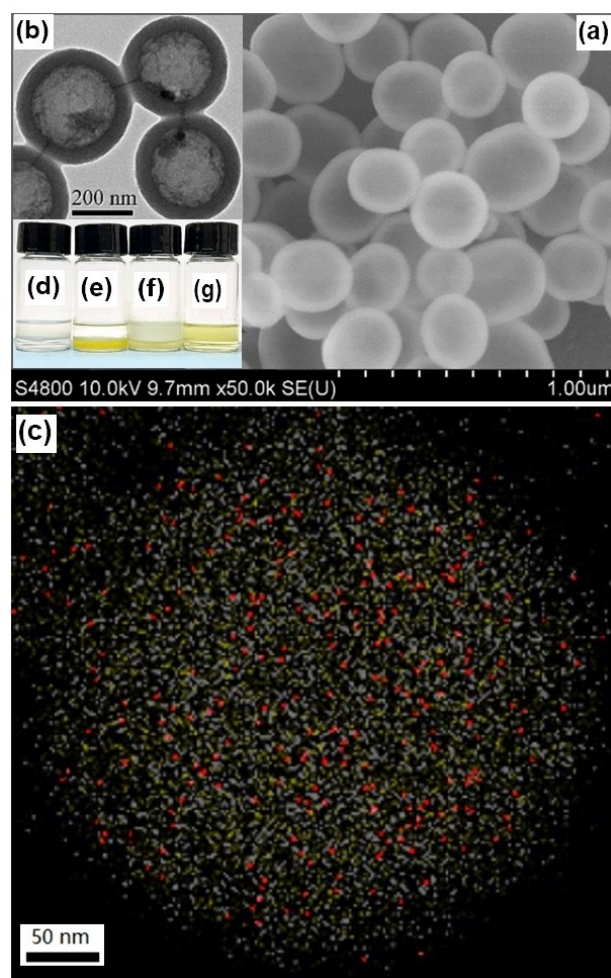


Figure 2. (a) SEM images of catalyst **5**, (b) TEM images of catalyst **5**, and (c) TEM image with the chemical mapping of **5** showing the distribution of Si (white) and Rh (red). Dispersive situations in CH_2Cl_2 /water (V/V = 1/2) co-solvents for **3** in upper water (d), for **5** in lower CH_2Cl_2 (e), for a mixture of **3** and **5** with **3** in upper water and **5** in below CH_2Cl_2 (f), and for a mixture of **3** and **5'** with both in upper water (g).

TEM image with a chemical mapping demonstrated that the rhodium centers in **5** were uniformly distributed (Figure 2c). Furthermore, the nitrogen adsorption-desorption isotherms of **5** also confirmed its mesoporous structure, since a typical IV character with an H_1 hysteresis loop was observed that was the same as those reported for hollow-shell-structured mesoporous silica (see Figure S7 of ESI).^[10c]

Catalytic Property

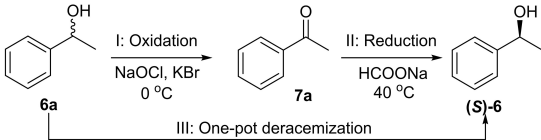
With the as-made catalysts **3** and **5** prepared, a series of control experiments based on two single-step reactions (I and II) and a cascade (III) were evaluated for the optimization of the redox deracemization, as shown in Table 1. In the evaluation of the single-step reaction stage, we found that the single-step oxidation (I) of the racemic 1-phenylethan-1-ol (**6a**) catalyzed by **3** at 0 °C could produce the intermediate acetophenone (**7a**) in a similar yield to that obtained with the homogeneous TEMPO, demonstrating a maintainable reactivity after the immobilization of TEMPO (entry 2 versus entry 1, Table 1). However, the single-step oxidation with a mixture of TEMPO plus Cp*RhTsDPEN or a mixture of **3** plus Cp*RhTsDPEN afforded **7a** with decreased yields relative to those catalyzed by just TEMPO or **3** (entries 3 and 4 versus entries 1 and 2, Table 1). This comparison indicated that the Cp*RhTsDPEN affected the reactivity of TEMPO.

In the case of the single-step reduction (II) of **7a**, the ATH catalyzed by **5** at 40 °C could also give (*S*)-1-phenylethan-1-ol (*(S)*-**6a**) in 97% yield and 98% ee, which was comparable to that attained with its homogeneous Cp*RhTsDPEN (entry 6 versus entry 5, Table 1). However, this ATH transformation with

the mixed TEMPO and Cp*RhTsDPEN gave a decreased yield and diminished ee when compared with that with the only Cp*RhTsDPEN (entry 7 versus entry 5, Table 1). Although this situation could be slightly improved in the reaction with the mixed TEMPO and supported **5** (entry 8 versus entry 5, Table 1), the still low yield and ee value demonstrated that the TEMPO also disturbed the reactivity and enantioselectivity of Cp*RhTsDPEN to a certain degree. Through the evaluation of two single-step reactions, a conclusion could be drawn, wherein the TEMPO and Cp*RhTsDPEN species are incompatible.

In the evaluation of the cascade reaction (III) stage, we compared three kinds of different dual catalysts systems for the model redox deracemizations of racemic **6a** in a one-pot manner. In the case of the unsupported TEMPO and Cp*RhTsDPEN as a dual catalysts system, we found that the cascade reaction gave the mixed **7a** (76% yield) and nearly racemic alcohols (23% yield) (entry 9, Table 1). This observation demonstrated that there was an obvious mutual deactivation behavior in a one-pot manner. This phenomenon indicated that two issues, the inner incompatible nature between TEMPO and Cp*RhTsDPEN discussed above and the outer disturbances coming from the aqueous components (NaOCl and KBr for the oxidation), imparted a negative influence on this redox deracemization in this one-pot process. In the case of the partly supported dual catalysts systems, it was found that the cascade reaction catalyzed by the integrated **3** and Cp*RhTsDPEN gave the final product (*(S)*-**6a**) with a similar result to that attained with the unsupported TEMPO and Cp*RhTsDPEN (entry 10 versus entry 9, Table 1). This finding indicated that the negative effect coming from the outer aqueous NaOCl could destroy the reduction process since the single-step reduction without the NaOCl and KBr gave the markedly enhanced (*S*)-**6a** (entry 10

Table 1. Optimizations of the dual catalysts used in the redox deracemization.^[a]



Entry	Reaction	Catalysts	7a , [%] Yield	(<i>S</i>)- 6a , [%] Yield [% ee]
1	I	TEMPO	97	/
2	I	3	97	/
3	I	TEMPO + [Rh]	79	/
4	I	3 + [Rh]	81	/
5	II	[Rh]	/	98 (98)
6	II	5	/	97 (98)
7	II	TEMPO + [Rh]	/	72 (91)
8	II	TEMPO + 5	/	85 (93)
9	III	TEMPO + [Rh]	76	23 (5)
10	III	3 + [Rh]	62	37 (5)
11	III	TEMPO + 5	17	82 (91)
12	III	3 + 5	trace	97 (98)

[a] Reaction conditions: For the reaction I, catalysts (1.0 mol% of TEMPO, and/or 1.0 mol% of Rh), **6a** (0.10 mmol), KBr (11.90 mg, 1 equivalents) and NaOCl (0.70 mL, 1.0 M, 7 equivalents) in 3.0 mL of CH₂Cl₂/H₂O (v/v = 1/2), 0 °C, 10 h. For reaction II, catalysts (1.0 mol% of Rh, and/or 1.0 mol% of TEMPO), **7a** (0.10 mmol), and HCOONa (15 equiv.) in 3.0 mL of CH₂Cl₂/H₂O (v/v = 1/2), 40 °C, 18 h. For cascade reaction III, dual catalysts (1.0 mol% of TEMPO, 1.0 mol% of Rh), **6a** (0.10 mmol), KBr (11.90 mg, 1 equivalents) and NaOCl (0.70 mL, 1.0 M, 7 equivalents) in 3.0 mL of CH₂Cl₂/H₂O (v/v = 1/2) at 0 °C for the first 10 h, followed by addition of HCOONa (10 equivalents) at 40 °C for the second 18 h. All yields were determined using ¹H-NMR spectroscopy and the ee values were determined using chiral HPLC analysis. [Rh] = Cp*RhTsDPEN.

versus entries 5 and 6, Table 1). This phenomenon could be further confirmed by a single-step parallel experiment, wherein the ATH of **7a** catalyzed by Cp*RhTsDPEN in the presence of NaOCl and KBr only provides (*S*)-**6a** with trace yield. Interestingly, this kind of outer disturbance could be markedly improved in the case of the integrated TEMPO and **5** as a dual catalysts system, since the cascade could provide (*S*)-**6a** in an 82% yield and 91% *ee*. This observation illustrated that the addition of the excess HCOONa could destroy the residual aqueous NaOCl component, thereby reducing the outer disturbances imparted on Cp*RhTsDPEN center and leading to an enhanced yield and enantioselectivity (entry 11 versus entries 9 and 10, Table 1). In the case of the supported **3** and **5** as a dual catalysts system, the cascade reaction could reach the reaction completion, providing (*S*)-**6a** in a 97% yield and 98% *ee*, which was similar to the corresponding two single-step transformations (entry 12 versus entries 2 and 6, Table 1). This finding demonstrated that the designed dual catalysts realized the efficient redox deracemization process from incompatibility to compatibility, indicating the advantage of the phase separation in this dual catalysts system.

To determine the phase separation-promoted redox deracemization, three aspects of the effecting factors were further investigated, as shown in Table 2. In the investigation of the role of the phase separation based on the hydrophilicity/hydrophobicity, the model one-pot redox deracemization of the racemic **6a** catalyzed by the integrated **3** and **5'** (a parallel analog of the catalyst **5** without the outer polymer-coating layer) was compared. It was found that a 68% yield (86% *ee*) of (*S*)-**6a** was observed, which was obviously lower than a 97% yield (98% *ee*) in the supported **3** and **5** dual catalysts system (entry 2 versus entry 1, Table 2). This comparison indicated a lack of the phase separation ability in this integrated **3** and **5'** dual catalysts system proven by an investigation of the dispersive situations in the mixed co-solvents (CH₂Cl₂/H₂O: v/v = 1:2). As shown in 2d–2g of Figure 2, catalyst **3** was hydrophilic with being highly dispersed in H₂O (Figure 2d), and **5** was hydrophobic with being highly dispersed in CH₂Cl₂ (Figure 2e), whereas catalysts **3** and **5** presented an obvious layer-isolated

behavior (Figure 2f). However, both catalysts **3** and **5'** were hydrophilic that were highly dispersed in the upper H₂O layer (Figure 2g). Due to no layer-isolated behavior in this integrated **3** and **5'** dual catalysts system, the *in-situ* generated oxidative ketone (**7a**) goes through the phase separation to enter the lower CH₂Cl₂ layer for the ATH transformation (a biphasic driving shift of **7a** into CH₂Cl₂ layer), thereby leading to a poor reactivity.

In the investigation of a biphasic driving force, we further tested the partition coefficient of the intermediate ketone (**7a**) and the racemic alcohol (**6a**) in the co-solvents (CH₂Cl₂/H₂O: v/v = 1:2). It was found that the partition coefficient of **7a** in the below CH₂Cl₂ layer is more than 99.9% detected by HPLC analysis, confirming that this phase separation driving force makes **7a** completely enter the organic layer for the second-step reduction. This demonstrated the obvious difference in the investigation of the hydrophilicity/hydrophobicity for the above two dual catalysts systems. Also, we analyzed the partition coefficient of the racemic **6a** since the unreacted residual **6a** could make the total *ee* value of (*S*)-**6a** to be diminished. The result showed that the partition coefficient of **6a** in a mixture of CH₂Cl₂ and H₂O is 85/15. Interestingly, the first-step oxidation reaction during this cascade process in the only H₂O as a solvent did not occur under the optimal reaction conditions,^[11a] wherein the *ee* value was still the same as that of the racemate (entry 3, Table 2). This finding demonstrated that, to avoid a diminished *ee* value of (*S*)-**6a** in this co-solvents system (CH₂Cl₂/H₂O: v/v = 1:2), the first-step oxidation during the cascade process must be converted completely, which might be an obligatory demand for high enantioselectivity. This finding indicated that a cascade directionality played a crucial function during this one-pot transformation.

In the investigation of the phase separation-promoted cascade directionality, we compared the model cascade reaction at the different reaction temperatures (entries 4 and 5, Table 2). It was found that the thermoresponsive polymer-coating layer in **5** was necessary because the cascade reaction either at 20 °C or 40 °C gave the final (*S*)-**6a** with the obviously decreased yields and *ee* values. This was attributed to the

Table 2. Identification of phase separation-promoted redox deracemization.^[a]

Entry	Catalysts	Solvent	X [°C]	[%] Yield and [% ee] ^[b]
1	3 + 5	CH ₂ Cl ₂ /H ₂ O (1/2)	0 °C	97/98
2	3 + 5'	CH ₂ Cl ₂ /H ₂ O (1/2)	0 °C	68/86
3	3 + 5	H ₂ O	0 °C	ND/0
4	3 + 5	CH ₂ Cl ₂ /H ₂ O (1/2)	20 °C	53/68
5	3 + 5	CH ₂ Cl ₂ /H ₂ O (1/2)	40 °C	45/56
6	3 + 5	toluene/H ₂ O (1/2)	0 °C	91/95
7	3 + 5	Et ₂ O/H ₂ O (1/2)	0 °C	38/93

[a] Reaction conditions: Catalysts (1.0 mol% of TEMPO, 1.0 mol% of Rh), **6a** (0.10 mmol), KBr (11.90 mg, 1 equivalent) and NaOCl (0.70 mL, 1.0 M, 7 equivalents) in 3.0 mL of solvents at X °C for the first 10 h, followed by addition of HCOONa (10 equivalents) at 40 °C for the second 18 h. [b] Yields were determined using ¹H-NMR spectroscopy and the *ee* values were determined using chiral HPLC analysis. ND = not detected.

swelling conformational state of the thermoresponsive polymer-coating layer in **5** at $>10^{\circ}\text{C}$ proven by a turbidity investigation of **5** (see Figure S8 of ESI).^[10c,13a] During this process, the first-step oxidation and the second-step reduction simultaneously proceeded. As a result, the partly final (*S*)-**6a** was repeatedly oxidized into **7a** for an not useful consumption of oxidative reagents, leading to an uncompleted conversion of racemic **6a** thereby a poor yield with *ee* value. It is noteworthy that, among those mixed co-solvents, a mixture of CH_2Cl_2 and H_2O was the optimal co-solvent system used in this one-pot

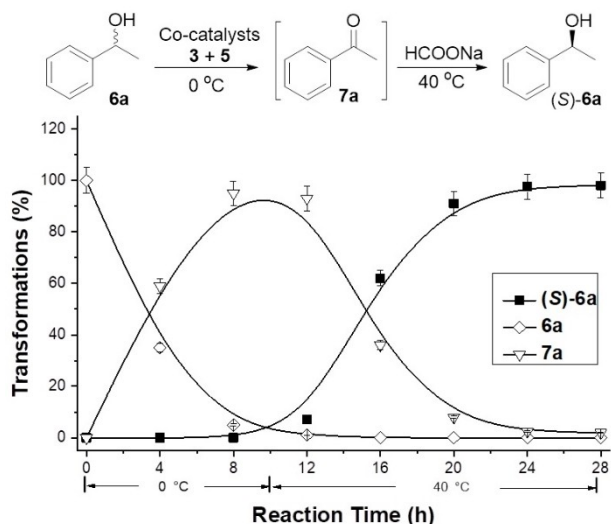


Figure 3. The time-course of the dual catalysts **3** and **5** for the redox deracemization of racemic 1-phenylethanol-1-ol (**6a**) (The error bars represent the standard deviation). The reaction was performed with 1.0 mol% of TEMPO in **3** and 1.0 mol% Rh in **5**, 1 equivalent of **6a**, in 3.0 mL of $\text{CH}_2\text{Cl}_2/\text{H}_2\text{O}$ ($v/v = 1/2$) containing 7 equivalents of NaOCl, 1 equivalent of KBr at 0°C for the first 10 h, followed by addition of 10.0 equivalent of HCOONa at 40°C for the second 18 h).

redox deracemization because of the highest yield and *ee* value (entry 1 versus entries 6 and 7, Table 2).

To clarify the role of the thermoresponsive polymer-coating layer of **5** in manipulating the phase separation-promoted cascade directionality during this one-pot redox deracemization process, a kinetic process by detecting the time-course of this supported dual catalysts system was also investigated, as shown in Figure 3. Initially, the oxidation of the racemic **6a** smoothly proceeds at 0°C as the concentration of **6a** rapidly decreases. After the transformation over the first 10 h, the intermediate **7a** reaches a maximum yield of 97%. Subsequently, after the addition of HCOONa at room temperature and the adjustment of the reaction temperature to 40°C , the ATH of **7a** occurs to sharply yield (*S*)-**6a** as the concentration of **7a** gradually decreases between 10 and 20 h. Finally, the reaction smoothly proceeds to afford (*S*)-**6a** in a 97% yield after a further 8 h. This investigation disclosed a controllable cascade directionality, which was comprised of an oxidation followed by the ATH process.

Based on the feasible one-pot redox deracemization process, a series of aryl-substituted secondary alcohols were further examined, as shown in Table 3. The results showed that all the tested achiral substrates could be steadily converted into the corresponding chiral products in high yields and enantioselectivities, which were comparable to those attained with the single-step enantioselective ATH transformation.^[14a] No significant stereoelectronic properties of the substituents on the aromatic rings were observed because their enantioselectivities with the electron-withdrawing (F, Cl, Br, and NO_2) or -donating substituents (MeO, and Me) on the aromatic rings were equally efficient (entries 2–5 versus entries 6–9). Furthermore, the one-pot redox deracemizations of the naphthyl-, furyl-, and thienyl-substituted substrates also produced the corresponding chiral products with high enantioselectivities (entries 10–12).

Table 3. One-pot redox deracemization of racemic secondary alcohols.^[a]

Entry	(<i>S</i>)- 6	Ar	[%] Yield ^[b]	[% <i>ee</i>] ^[c]
1	(<i>S</i>)- 6a	Ph	97	98
2	(<i>S</i>)- 6b	4-FPh	83	93
3	(<i>S</i>)- 6c	4-ClPh	81	91
4	(<i>S</i>)- 6d	4-BrPh	84	93
5	(<i>S</i>)- 6e	4- NO_2 Ph	77	83
6	(<i>S</i>)- 6f	4-MePh	87	90
7	(<i>S</i>)- 6g	3-MePh	93	90
8	(<i>S</i>)- 6h	4-OMePh	93	93
9	(<i>S</i>)- 6i	3-OMePh	84	95
10	(<i>S</i>)- 6j	2-naphthyl	93	92
11	(<i>S</i>)- 6k	2-furyl	78	96
12	(<i>S</i>)- 6l	2-thienyl	76	96

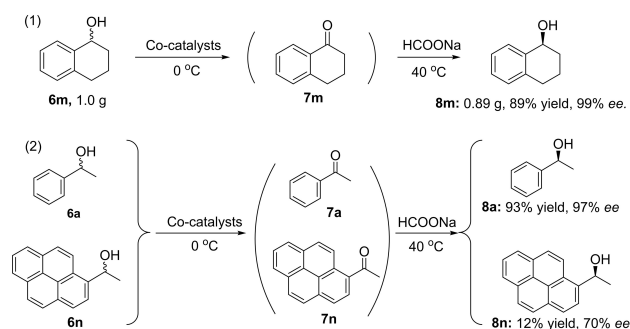
[a] Reaction conditions: Dual catalysts (1.0 mol% of TEMPO, 1.0 mol% of Rh), **6a** (0.10 mmol), KBr (11.90 mg, 1 equivalent) and NaOCl (0.70 mL, 1.0 M, 7 equivalents) in 3.0 mL of $\text{CH}_2\text{Cl}_2/\text{H}_2\text{O}$ ($v/v = 1/2$) at 0°C for the first 10 h, followed by addition of HCOONa (10 equivalents) at 40°C for the second 18 h.

[b] Isolated yields. [c] The *ee* values were determined using chiral HPLC analysis (see Figure S9 and Figure 11 of ESI).

In addition to the one-pot redox deracemization studied in Table 3, the preparation of the other chiral alcohols used in this supported dual catalysts system was also performed, as shown in Scheme 3. It was found that a gram-scale 1,2,3,4-tetrahydronaphthalen-1-ol (**6m**) could be converted into (*S*)-**6m** in 89% yield and 99% ee (equation 1). Moreover, the one-pot redox deracemization with the large-sized 1-(pyren-1-yl)ethan-1-ol (**6n**) and small-sized **6a** as the mixed substrates mainly gave (*S*)-**6a** (93% yield and 97% ee) along with a small amount of (*S*)-**6n** (equation 2). However, a normal reduction of **7n** catalyzed by the homogeneous Cp*RhTsDPEN gave (*S*)-**6n** in 91% yield and 93% ee. This observation suggested that the reaction with the large-sized substrate is more difficult to pass through the nanopores than with the small-sized substrate thereby a poor reactivity.

Catalyst's Recyclability

Another consideration for the design of this supported dual catalysts system expects high recyclability, wherein the dual catalysts could be recovered and recycled *via* a simple filtration. As shown in Figure 4, in a consecutive one-pot redox deracemization of **6a**, we found that the supported dual catalysts could



Scheme 3. Preparation of (*S*)-1,2,3,4-tetrahydronaphthalen-1-ol and investigation of the substrate selectivity in the redox deracemization.

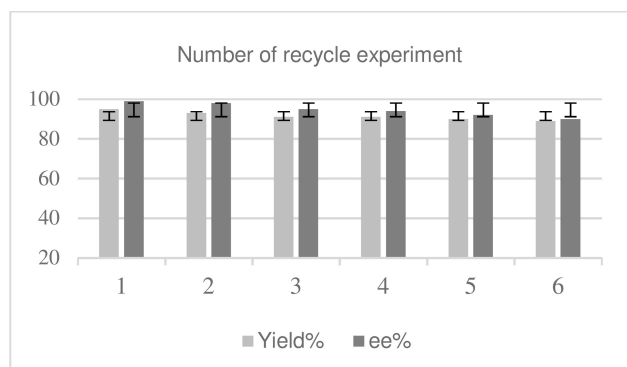


Figure 4. Reusability of the dual catalysts used in the redox deracemization of **6a** (The error bars represent the standard deviation).

be recycled six times. In the sixth run, the supported dual catalysts could still give the chiral (*S*)-**6a** in an 86% yield with a 90% ee value (see Table S1 and Figure S10 of ESI).

Conclusion

In conclusion, through the use of two different types of silica nanoparticles as dual-supports, we have successfully immobilized TEMPO onto the outer surface of a silica nanoparticles, and the Rh/diamine species in the nanochannels of silica shell of another mesoporous silica. By integrating them into a dual catalysts system, an efficient redox deracemization of secondary alcohols is realized, where the TEMPO species catalyzes the oxidation of racemic secondary alcohols into ketones, and the chiral Rh/diamine species converts the *in-situ* generated intermediate to the corresponding enantioenriched secondary alcohols. As presented in this study, this dual catalysts system can efficiently solve the problem of mutual interactions between TEMPO and Rh/diamine of dual-species, providing various chiral products in high yields and enantioselectivities. Furthermore, a time-course study discloses a sequential reaction sequence in the one-pot redox deracemization process. The presented study also offers an avenue for the exploration of multi-step sequential enantioselective organic transformation through the use of this kind of integrated dual catalysts system.

Experimental Section

Preparation of Catalyst 3

In a typical synthesis. The SiO₂@NPs (1) (1.0 g) were dispersed in 20.0 mL of dry toluene, and 3-(triethoxysilyl)propanamine (200.0 mg, 0.90 mmol) was added to this suspension at room temperature. The resulting mixture was stirred at 25 °C for 24 h. After the filtration, the collected white solid (2) (1.01 g) was suspended in 20.0 mL of dry methanol, 4-oxo-TEMPO (0.34 g, 2.0 mmol), and NaBH₃CN (0.13 g, 2.0 mmol) in dry methanol (10 mL) was added, and the resulting mixture was stirred at 25 °C for 24 h. The mixture was filtered and then washed with excess water and methanol. After Soxhlet extraction for 24 h in CH₂Cl₂, the solid was dried at room temperature under vacuum overnight to afford **3** (1.03 g) as a white powder. Thermogravimetric analysis (TG) showed the TEMPO-loadings were 3.45% (0.22 mmol, 34.57 mg) per gram of catalyst (**3**). ¹³C CP/MAS NMR (161.9 MHz): 70.5 (–CH₂N⁺– in the surfactant cetyltrimethylammonium bromide (CTAB) moiety), 65.3–59.4 (–C– and –CH– of cyclic alkyl carbon atoms connected to the nitrogen atom), 57.3 (–N⁺(CH₃)₃ in the surfactant cetyltrimethylammonium bromide (CTAB) moiety), 46.5 (–SiCH₂CH₂CH₂N–), 33.3 (–CH₂– in CTAB moiety), 29.7 (–SiCH₂CH₂CH₂N–, and –CH₂CH₂N⁺– in CTAB moiety), 26.1 (–CH₂– of cyclic alkyl carbon atoms and CH₃CH₂– in CTAB moiety), 19.5 (CH₃– in cyclic moiety, and CH₃– in CTAB moiety), 12.5 (–SiCH₂–). ²⁹Si MAS/NMR (79.4 MHz): Q² (δ = –89.9 ppm), Q³ (δ = –102.0 ppm), Q⁴ (δ = –112.5 ppm).

Preparation of Catalyst 5

In a typical synthesis. (First step for the polymerization) The obtained Vinyl@SiO₂@HSMSNPs (**4**) (0.50 g) were dispersed in 10 mL of

distilled DMSO under a nitrogen atmosphere and acrylamide (0.10 g, 1.41 mmol), acrylonitrile (0.019 g, 0.36 mmol), and 2,2-azobisisobutyronitrile (AIBN) (6.64 mg, 2% mol) added to the resulting solution at room temperature. After degassing the reaction mixture *via* three freeze-pump-thaw cycles, the flask was placed into an oil bath to polymerize at 60 °C for 6 h. (Second step for the coordination) After cooling to room temperature, the resulting white solid 4' (0.56 g) was collected by centrifugation and suspended in 20.0 mL of dry CH₂Cl₂. Then, 50.0 mg of (Cp**Rh*Cl₂)₂ (0.086 mmol) was added to this suspension, and the resulting mixture was stirred at 40 °C for 12 h. After Soxhlet extraction for 24 h in CH₂Cl₂, the resulting solid was dried at room temperature under vacuum overnight to afford catalyst 5 (0.57 g) as a light-yellow powder. Inductively coupled plasma optical emission spectroscopy (ICP-OES) showed that the Rh-loading was 8.63 mg (0.084 mmol) per gram of catalyst. ¹³C CP/MAS NMR (161.9 MHz): 192.4 (C=O), 158.1–118.3 (C of Ar, –CN, and Ph), 99.4 (–CH of Cp*), 70.7, 66.9 (–NCH₂CHN–), 65.1–60.7 (–NCH₂ in CTAB), 60.4–55.0 (–CHCN and –CH CONH₂ in the polymer), 39.8–28.2 (–CH₂– in polymer, and –CH₂– in CTAB), 26.9 (–CH₂Ar), 13.0 (–CH₃ in Cp*), 8.4 (–CH₂Si and –CH₃ in CTAB) ppm. ²⁹Si MAS/NMR (79.4 MHz): T² (δ = –59.0 ppm), T³ (δ = –66.9 ppm), Q² (δ = –93.0 ppm), Q³ (δ = –102.7 ppm), Q⁴ (δ = –110.5 ppm). Elemental analysis (%): found, C 25.21, H 2.11, N 2.13, S 0.46.

General Procedure for the Redox Deracemization Process

A typical procedure was as follows. A suspension of catalysts 3 (4.55 mg, 1.0 mol% of TEMPO, based on TG analysis) and 5 (11.92 mg, 1.0 mol% of Rh, based on ICP analysis), and alcohols (0.10 mmol) in 1.0 mL of CH₂Cl₂ was added to the 2.0 mL of an aqueous solution containing KBr (11.90 mg, 1 equivalent) and NaOCl (0.70 mL, 1.0 M, 7 equivalents) in a 10.0 mL round-bottom flask at 0 °C. The resulting mixture was then stirred at 0 °C for 6–12 h. After the completion of the oxidation reaction detected by TLC, HCO₂Na (1.0 mmol) was added to this suspension, and the resulting mixture was stirred at 40 °C for 6–24 h. During this period, the reaction was monitored by TLC. After completion of the reaction, the catalysts were separated by centrifugation (10,000 rpm) for the recycling experiment. The aqueous solution was extracted with ethyl ether (3 × 3.0 mL). The combined ethyl ether extracts were washed with aqueous Na₂CO₃ and then dehydrated with Na₂SO₄. After evaporation of the solvent, the resulting residue was purified by silica gel flash column chromatography to afford the desired product. The *ee* values were determined using HPLC analysis using a UV-Vis detector and Daicel chiral-cel column (Φ 0.46 × 25 cm).

Acknowledgements ((optional))

We are grateful to the China National Natural Science Foundation (22071154, 22001171), and the Shanghai Sciences and Technologies Development Fund (20070502600), and Shanghai Sailing Program (2020YF1435200) for financial supports.

Conflict of Interest

The authors declare no conflict of interest.

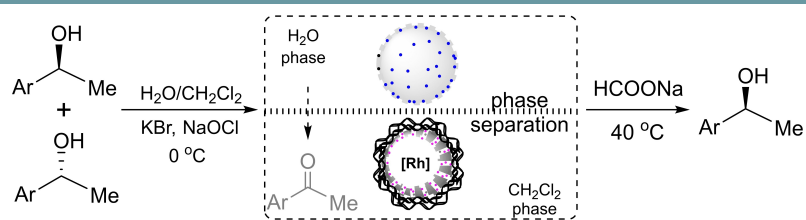
Keywords: Asymmetric catalysis · Deracemization · Heterogeneous catalysis · Mesoporous material · Supported catalysts

- [1] a) M. Rachwalski, N. Vermuea, F. P. J. T. Rutjes, *Chem. Soc. Rev.* **2013**, *42*, 9268–9282; b) S. Servi, D. Tessaro, G. Pedrocchi-Fantoni, *Coord. Chem. Rev.* **2008**, *252*, 715–726.
- [2] a) Q. Shi, J. Ye, *Angew. Chem. Int. Ed.* **2020**, *59*, 2–6; *Angew. Chem.* **2020**, *132*, 2–2; b) N. Y. Shin, J. M. Ryss, X. Zhang, S. J. Miller, R. R. Knowles, *Science* **2019**, *366*, 364–369; c) A. Trçster, A. Bauer, C. Jandl, T. Bach, *Angew. Chem. Int. Ed.* **2019**, *58*, 3538–3541; *Angew. Chem.* **2019**, *131*, 3576–3579; d) A. Hçlzl-Hobmeier, A. Bauer, A. V. Silva, S. M. Huber, C. Bannwarth, T. Bach, *Nature* **2018**, *564*, 240–243.
- [3] a) C. J. Dunsmore, R. Carr, T. Fleming, N. J. Turner, *J. Am. Chem. Soc.* **2006**, *128*, 2224–2225; b) D. Ghislieri, A. P. Green, M. Pontini, S. C. Willies, I. Rowles, A. Frank, G. Grogan, N. J. Turner, *J. Am. Chem. Soc.* **2013**, *135*, 10863–10869.
- [4] a) L. C. Sögütöglu, R. R. E. Steendam, H. Meekes, E. Vlieg, F. P. J. T. Rutjes, *Chem. Soc. Rev.* **2015**, *44*, 6723–6732; b) M. Guillot, J. Meester, S. Huynen, L. Collard, K. Robeyns, O. Riant, T. Leyssens, *Angew. Chem. Int. Ed.* **2020**, *59*, 11303–11306; *Angew. Chem.* **2020**, *132*, 11399–11402; c) C. Rougeot, J. E. Hein, *Org. Process Res. Dev.* **2015**, *19*, 1809–1819.
- [5] a) N. J. Turner, *Curr. Opin. Chem. Biol.* **2010**, *14*, 115–121; b) C. C. Gruber, I. Lavandera, K. Faber, W. Kroutil, *Adv. Synth. Catal.* **2006**, *348*, 1789–1805; c) K. Faber, *Chem. Eur. J.* **2001**, *7*, 5004–5010.
- [6] a) A. D. Lackner, A. V. Samant, F. D. Toste, *J. Am. Chem. Soc.* **2013**, *135*, 14090–14093; b) Y. Ji, L. Shi, M. W. Chen, G. S. Feng, Y. G. Zhou, *J. Am. Chem. Soc.* **2015**, *137*, 10496–10499; c) M. Wan, S. Sun, Y. Li, L. Liu, *Angew. Chem. Int. Ed.* **2017**, *56*, 5116–5120; *Angew. Chem.* **2017**, *129*, 5198–5202.
- [7] a) J. N. Zhou, Q. Fang, Y. H. Hu, L. Y. Yang, F. F. Wu, L. J. Xie, J. Wu, S. Li, *Org. Biomol. Chem.* **2014**, *12*, 1009–1017; b) D. W. Robertson, J. H. Krushinski, R. W. Fuller, J. D. Leander, *J. Med. Chem.* **1988**, *31*, 1412–1417; c) A. Träff, R. Lihammar, J. A. Bäckvall, *J. Org. Chem.* **2011**, *76*, 3917–3921; d) Y. Gao, K. B. Sharpless, *J. Org. Chem.* **1988**, *53*, 4081–4084; e) H. Kakei, T. Nemoto, T. Ohshima, M. Shibasaki, *Angew. Chem. Int. Ed.* **2004**, *43*, 317–320; *Angew. Chem.* **2004**, *116*, 321–324; f) Y. Fujima, M. Ikunaka, T. Inoue, J. Matsumoto, *Org. Process Res. Dev.* **2006**, *10*, 905–913; g) A. Bosak, I. Gazić Smilović, G. Šinko, V. Vinković, Z. Kovarik, *J. Med. Chem.* **2012**, *55*, 6716–6723; h) L. Huang, W. Shan, Q. Zhou, J. Xie, K. Lai, X. Li, *Bioorg. Med. Chem. Lett.* **2014**, *24*, 249–253.
- [8] a) G. R. Allan, A. J. Carnell, *J. Org. Chem.* **2001**, *66*, 6495–6497; b) D. Kato, S. Mitsuda, H. Ohta, *Org. Lett.* **2002**, *4*, 371–373; c) D. Kato, S. Mitsuda, H. Ohta, *J. Org. Chem.* **2003**, *68*, 7234–7242; d) C. V. Voss, C. C. Gruber, K. Faber, T. Knaus, P. Macheroux, W. Kroutil, *J. Am. Chem. Soc.* **2008**, *130*, 13969–13972; e) C. V. Voss, C. C. Gruber, W. Kroutil, *Angew. Chem. Int. Ed.* **2008**, *47*, 741–745; *Angew. Chem.* **2008**, *120*, 753–757; f) L. Ou, Y. Xu, D. Ludwig, J. Pan, J. H. Xu, *Org. Process Res. Dev.* **2008**, *12*, 192–195; g) Y. P. Xue, Y. G. Zheng, Y. Q. Zhang, J. L. Sun, Z. Q. Liu, Y. C. Shen, *Chem. Commun.* **2013**, *49*, 10706–10708; h) T. Saravanan, S. Jana, A. Chadha, *Org. Biomol. Chem.* **2014**, *12*, 4682–4690; i) C. V. Voss, C. C. Gruber, W. Kroutil, *Angew. Chem. Int. Ed.* **2008**, *47*, 741–745; *Angew. Chem.* **2008**, *120*, 753–757; j) C. V. Voss, C. C. Gruber, K. Faber, T. Knaus, P. Macheroux, W. Kroutil, *J. Am. Chem. Soc.* **2008**, *130*, 13969–13972.
- [9] a) G. R. A. Adair, J. M. J. Williams, *Chem. Commun.* **2005**, 5578–5579; b) G. R. A. Adair, J. M. J. A. Williams, *Chem. Commun.* **2007**, 2608–2009; c) Y. Shimada, Y. Miyake, H. Matsuzawa, Y. Nishibayashi, *Chem. Asian J.* **2007**, *2*, 393–396; d) P. Qu, M. Kuepfert, S. Jockusch, M. Weck, *ACS Catal.* **2019**, *9*, 2701–2706; e) W. Kroutil, K. Faber, *Tetrahedron: Asymmetry* **1998**, *9*, 2901–2913.
- [10] a) F. Gelman, J. Blum, D. Avnir, *Angew. Chem. Int. Ed.* **2001**, *40*, 3647–3649; *Angew. Chem.* **2001**, *113*, 3759–3761; b) Y. Ueda, H. Ito, D. Fujita, M. Fujita, *J. Am. Chem. Soc.* **2017**, *139*, 6090–6093; c) F. Chang, S. Wang, Z. Zhao, L. Wang, T. Cheng, G. Liu, *ACS Catal.* **2019**, *10*, 10381–10389; d) Y. Yang, X. Liu, X. Li, J. Zhao, S. Bai, J. Liu, Q. Yang, *Angew. Chem. Int. Ed.* **2012**, *51*, 9164–9168; *Angew. Chem.* **2012**, *124*, 9298–9302; e) P. Qu, M. Kuepfert, E. Ahmed, F. Liu, M. Weck, *Eur. J. Inorg. Chem.* **2021**, 1420–1427; f) R. Poli, *Site Isolation for Non-orthogonal Tandem Catalysis in Confined Nanospaces in Effects of nanoconfinement on Catalysis*, (Eds.: R. Poli), Springer International Publishing AG, **2017**, pp 209–258.
- [11] a) T. Fe, H. Fischer, S. Bachmann, K. Albert, C. Bolm, *J. Org. Chem.* **2001**, *66*, 8154–8159; b) H. Ahmad Beejapur, Q. Zhang, K. Hu, L. Zhu, J. Wang, Z. Ye, *ACS Catal.* **2019**, *9*, 2777–2830; c) C. Chen, N. Kang, T. Xu, D.

- Wang, L. Ren, X. Q. Guo, *Nanoscale* **2015**, *7*, 5249–5261; d) P. L. Anelli, C. Biffi, F. Montanari, S. Quici, *J. Org. Chem.* **1987**, *52*, 2559–2562.
- [12] O. Kröcher, R. A. Köppel, M. Fröba, A. Baiker, *J. Catal.* **1998**, *178*, 284–298.
- [13] a) J. Seuring, S. Agarwal, *Macromolecules* **2012**, *45*, 3910–3918; b) I. Mathakiya, V. Vangani, A. K. Rakshit, *J. Appl. Polym. Sci.* **1998**, *69*, 217–228; c) D. E. Bergbreiter, P. L. Osburn, A. Wilson, E. M. Sink, *J. Am. Chem. Soc.* **2000**, *122*, 9058–9064.
- [14] a) X. F. Wu, X. H. Li, A. Zanotti-Gerosa, A. Pettman, J. Liu, A. J. Mills, J. L. Xiao, *Chem. Eur. J.* **2008**, *14*, 2209–2222; b) X. F. Wu, J. Liu, D. D. Tommaso, J. A. Iggo, C. R. Catlow, J. Bacsá, J. L. Xiao, *Chem. Eur. J.* **2008**, *14*, 7699–7715; c) P. N. Liu, J. G. Deng, Y. Q. Tu, S. H. Wang, *Chem. Commun.* **2004**, 2070–2071; d) N. A. Cortez, G. Aguirre, M. Parra-Hake, R. Somanathan, *Tetrahedron Lett.* **2009**, *50*, 2282–2291; e) T. Ikariya, A. J. Blacker, *Acc. Chem. Res.* **2007**, *40*, 1300–1308; f) J. E. D. Martins, G. J. Clarkson, M. Wills, *Org. Lett.* **2009**, *11*, 847–850.

Manuscript received: May 19, 2021
Revised manuscript received: July 20, 2021
Version of record online: ■■■, ■■■■

FULL PAPERS



Redox deracemization to chiral alcohols: A supported dual catalysts system by overcoming the mutually deactivated TEMPO and Rh/diamine dual-species is developed. Dual

catalysts perform an efficient phase separation-promoted redox deracemization of secondary alcohols to provide various chiral alcohols with high yields and enantioselectivities.

Z. Zhao, C. Wang, Q. Chen, Y. Wang, R. Xiao, C. Tan*, Prof. G. Liu*

1 – 10

Phase Separation-Promoted Redox Deracemization of Secondary Alcohols over a Supported Dual Catalysts System

